



Global Biogeochemical Cycles

RESEARCH ARTICLE

10.1002/2013GB004678

Key Points:

- Tight TA-salinity relationship and predictable TA in oligotrophic open oceans
- NTA informs the alkalinity addition/removal in ocean margins and inland seas
- The intercept of TA-salinity regression could bias the river TA concentration

Supporting Information:

- Readme
- Figure S1
- Figure S2

Correspondence to:

Z.-P. Jiang,
zpjia@zju.edu.cn

Citation:

Jiang, Z.-P., T. Tyrrell, D. J. Hydes, M. Dai, and S. E. Hartman (2014), Variability of alkalinity and the alkalinity-salinity relationship in the tropical and subtropical surface ocean, *Global Biogeochem. Cycles*, 28, 729–742, doi:10.1002/2013GB004678.

Received 21 JUN 2013

Accepted 16 JUN 2014

Accepted article online 21 JUN 2014

Published online 17 JUL 2014

Variability of alkalinity and the alkalinity-salinity relationship in the tropical and subtropical surface ocean

Zong-Pei Jiang^{1,2}, Toby Tyrrell¹, David J. Hydes¹, Minhan Dai³, and Susan E. Hartman¹

¹National Oceanography Centre, Southampton, University of Southampton, Southampton, UK, ²Ocean College, Zhejiang University, Hangzhou, China, ³State Key Laboratory of Marine Environmental Science, Xiamen University, Xiamen, China

Abstract The variability of total alkalinity (TA) and its relationship with salinity in the tropical and subtropical surface ocean were examined using data collected in various marine environments from a ship of opportunity. In the open ocean regions of the Atlantic, Pacific, and Indian Oceans, sea surface TA variability was observed to be mainly controlled by the simple dilution or concentration (SDC) effect of precipitation and evaporation, and the measured concentrations of TA agreed well with those predicted from salinity and temperature. Non-SDC changes in alkalinity in ocean margins and inland seas were examined by comparing the salinity-normalized alkalinity with that of the open ocean end-member. Non-SDC alkalinity additions to the western North Atlantic margin, eastern North Pacific margin, and Mediterranean Sea were identified, which mainly resulted from river inputs and shelf currents. In contrast, removal of TA through formation and sedimentation of calcium carbonate was observed to be an important control in the Red Sea. The concentration of the river end-member can only be reliably derived from the y intercept of TA-S regression (TA_{S0}) in river-dominated systems such as estuaries and river plumes. In coastal regions where other processes (evaporation, shelf currents, upwelling, calcification, etc.) are more influential, TA_{S0} can significantly deviate from the river water concentration and hence be an unreliable indicator of it. Negative values of TA_{S0} can result from non-SDC TA removal at the low salinity end (relative to the salinity of the oceanic end-member) and/or non-SDC TA addition at high salinities (as occurs in the Mediterranean Sea).

1. Introduction

Total alkalinity (TA) is an important variable in the study of the marine carbonate system and calcium carbonate ($CaCO_3$) cycling in the ocean [Brewer *et al.*, 1975; Feely *et al.*, 2004; Sarmiento *et al.*, 2002]. It is defined as the numbers of moles of hydrogen ion equivalent to the excess of proton acceptors over proton donors in 1 kg of seawater [Dickson, 1981, 1992; Dickson *et al.*, 2007]. By expanding Dickson's definition of TA to explicitly include the requirement of electroneutrality of aqueous solutions, Wolf-Gladrow *et al.* [2007] derived an alternative expression for TA in terms of conservative species. It is evident from this "explicit conservative" expression that TA is conservative (in gravimetric units, e.g., $\mu\text{mol kg}^{-1}$) with respect to mixing and changes in temperature and pressure, and this expression is especially well suited to derive alkalinity changes due to biogeochemical processes such as precipitation and dissolution of carbonates or uptake of various nutrients by microalgae (for details see Wolf-Gladrow *et al.* [2007]).

In the surface ocean, the global distribution of TA generally matches that of salinity (S) because TA in the open ocean is mainly controlled by freshwater addition or removal, which is reflected by salinity changes [Lee *et al.*, 2006; Millero *et al.*, 1998]. In the tropical and subtropical open ocean, changes in salinity account for more than 80% of the surface TA variability [Millero *et al.*, 1998]. In high-latitude regions, convective mixing of TA-rich deep water is an important factor affecting surface TA. This process can be indicated by the changes in sea surface temperature (SST): the intensified convection during the cooling season acts to increase the surface TA concentration, while little convective mixing occurs during summertime when SST is high [Lee *et al.*, 2006; Millero *et al.*, 1998]. Using salinity and SST as proxies for the main processes inducing surface TA variations in the open ocean, Lee *et al.* [2006] split the global ocean into five regimes, for each of which these authors proposed empirical algorithms to estimate the surface TA concentrations (with an average uncertainty of $\pm 8.1 \mu\text{mol kg}^{-1}$). Meanwhile, the concentration of TA can also be modulated by various biogeochemical processes, e.g., precipitation and dissolution of $CaCO_3$ [Bates *et al.*, 1996; Harlay *et al.*, 2010, 2011],

uptake and release of nutrients [Brewer and Goldman, 1976; Wolf-Gladrow et al., 2007], and anaerobic processes [Chen, 2002]. Moreover, TA variability in coastal environments is more complex due to effects of riverine inputs, shelf currents, upwelling, groundwater, and biological processes [Abril et al., 2003; Cai et al., 2010; Cao et al., 2011; Chen, 2002; Friis et al., 2003; Liu et al., 2012].

Identifying the controlling mechanisms of TA variability in different marine environments is important for understanding marine biogeochemistry and to work out how TA data can be used to diagnose important processes. Such understanding may also be useful in the context of the impact of CaCO_3 cycling from ocean acidification, i.e., the decreases in pH and saturation state of CaCO_3 (Ω) in the ocean [Doney, 2009; Doney et al., 2009; Orr et al., 2005]. Moreover, understanding the TA-S relationship is important both for estimating the end-member properties from field observations (two-end-member regression or multiple-end-member analysis) and calculating in situ biogeochemically induced changes (by comparing measurements to values predicted from conservative mixing).

Taking advantage of the wide sampling coverage of a ship of opportunity (SOO, or volunteer observing ship), here we take a detailed look at the surface TA distribution in various characteristic oceanographic regions spanning open ocean, ocean margins, and inland seas. The measured concentrations of TA in our study were compared to historical measurements archived in the Carbon Dioxide Information Analysis Center (CDIAC, <http://cdiac.ornl.gov/oceans/>), as well as to values estimated from empirical algorithms [Lee et al., 2006]. Based on this comparative study across a wide range of environments, the mechanisms controlling TA variability were examined in different marine environments, with special attention paid to controls on the y intercept of the TA-salinity regression (TA_{50}). A generally applicable theoretical framework is developed that advances our understanding of how TA, TA_{50} , and salinity-normalized TA (NTA) respond to the combined effects of simple dilution or concentration (SDC) and non-SDC processes. NTA was used as an indicator pinpointing the presence of non-SDC processes, and the possible sources of any non-SDC changes were investigated.

2. Methodology

2.1. Sampling, Measurement, and External Data

A low-maintenance automatic system, named the Swire National Oceanography Centre Monitoring System (SNOMS), was operated on the SOO M/V *Pacific Celebes* to observe CO_2 -related variables in the surface ocean (SST, salinity, dissolved oxygen, and partial pressure of CO_2) from June 2007 to March 2012 [Hydes et al., 2013; Jiang et al., 2014]. In addition to the automated underway measurements, discrete samples for salinity and TA ($n = 717$) were collected on a daily basis when the system was in operation. These samples were taken from the nontoxic seawater supply to the ship's freshwater generator, which was pumped from an intake at about 5 m below the sea surface. Salinity samples were collected in 100 mL borosilicate glass bottles. Samples for TA were collected in 250 mL borosilicate glass bottles (Schott Duran) and poisoned with 50 μL of saturated HgCl_2 solution to prevent biological alteration during storage [Dickson et al., 2007]. A headspace of 2.5 mL was left to allow for water expansion and the bottles were sealed using greased ground glass stoppers to ensure they remained gas-tight [Dickson et al., 2007]. These samples were analyzed under stable laboratory conditions at the National Oceanography Centre, Southampton. The salinity was measured using a Guildline Autosol salinometer with an accuracy of ± 0.002 . The measurements of TA were made using a VINDTA 3C (Marianda, Germany), by HCl titration of ~ 100 mL samples with a pH half-cell electrode (Orion, Ross, USA) and an Ag/AgCl reference electrode (Metrohm, Switzerland). The precision of TA measurement was estimated to be $\pm 1.5 \mu\text{mol kg}^{-1}$, and the accuracy was assured by calibration against Certified Reference Materials from Dr. Andrew Dickson (Scripps Institution of Oceanography). The SNOMS data are available from the CDIAC website (<http://cdiac.ornl.gov/oceans/>) [Hydes et al., 2012].

As shown in Figure 1, the ship traveled around the globe 4 times between June 2007 and March 2009: from Canada across the North Atlantic, through the Mediterranean and Red Sea, around India to Indonesia, across the equatorial Pacific, through the Panama Canal into the Gulf of Mexico, and then back to Canada. From March to September 2009, the ship traveled along one triangular route from Indonesia to North America via the Cape of Good Hope. After October 2009, the ship changed route to trade between Australia, New Zealand, and North America. The wide spatial coverage of sampling positions along the ship's route (Figure 1) thus provides a good opportunity to examine the distribution and variability of TA and its relationship with salinity in different environmental settings.

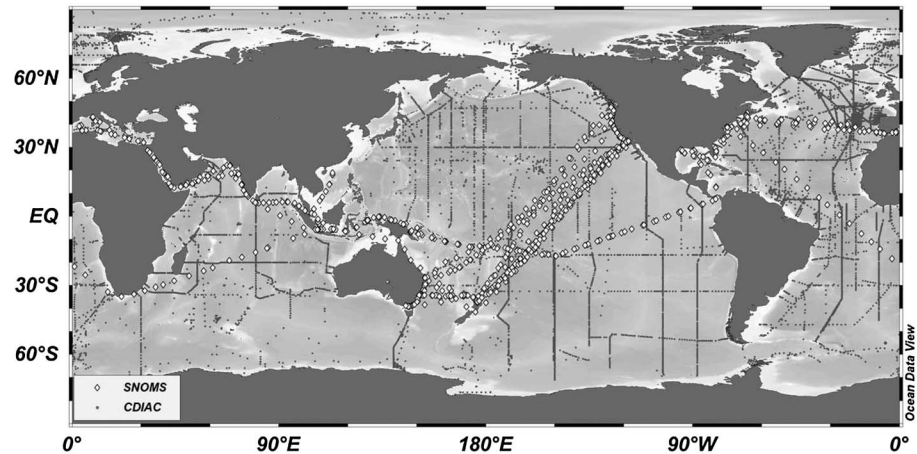


Figure 1. Sampling positions during the SNOMS project from 2007–2012 (open diamonds) and the historical measurements from the Carbon Dioxide Information Analysis Center (gray dots). Figure produced using Ocean Data View [Schlitzer, 2011].

In order to compare the SNOMS data to previous measurements and to better constrain the oceanic end-members, historical data were downloaded from CDIAC (Figure 1), including data sets from several data synthesis projects such as Global Ocean Data Analysis Project (v1.1) [Key *et al.*, 2004], Carbon dioxide in the Atlantic Ocean (v1.2) [Tanhua *et al.*, 2008], Pacific Ocean interior carbon [Suzuki *et al.*, 2013], and cruise data from the Global Coastal Program in the North American West and East Coasts [Feely and Sabine, 2011; Wanninkhof *et al.*, 2011] and the Mediterranean Sea [Schneider and Roether, 2007; Tanhua *et al.*, 2012]. Surface data were selected from waters up to 20 m depth in the (sub)tropics (30°S–30°N) and 30 m depth in regions with a latitude higher than 30° [Lee *et al.*, 2006].

2.2. Combined Effects of Simple Dilution or Concentration (SDC) and Non-SDC Processes

The alkalinity of a particular water parcel can be considered as being the result of conservative mixing of different components (TA_{mix}) together with an additional change due to biogeochemical processes (ΔTA_{bgc}):

$$TA = TA_{mix} + \Delta TA_{bgc} \quad (1)$$

Mixing usually affects salinity (unless the mixed-together components have identical salinity), whereas biogeochemical changes of ΔTA_{bgc} (e.g., precipitation and dissolution of $CaCO_3$, uptake and release of nutrients) result in negligible change in salinity. As values of ΔTA_{bgc} (usually a few to tens of $\mu mol\ kg^{-1}$) are much smaller than the mean concentration of TA [Sarmiento and Gruber, 2006], TA_{mix} tends to have a larger impact on the variability of TA. Therefore, TA is commonly observed to exhibit an approximately linear relationship with salinity:

$$TA = slope * S + TA_{S0} \quad (2)$$

where TA_{S0} is the y intercept of the TA-S regression. Extrapolation of equation (2) is widely used to estimate TA at salinity values where TA has not been measured. A typical example of this application is to use TA_{S0} to estimate the TA concentration of the fresh water end-member. However, regressions of the observational data sometimes generate negative y intercepts (e.g., in the Indian Ocean [Millero *et al.*, 1998] and in the Mediterranean Sea as discussed below in section 3.4). It is thus interesting to investigate how SDC and non-SDC processes combined to control the TA-S relationship and TA_{S0} .

Specific alkalinity, defined as the ratio of alkalinity to chlorinity, has been used in the past to compare alkalinity from different locations and depths; to identify the production of $CaCO_3$; and to characterize water masses [Koczy, 1956; Park, 1966, 1968]. In a similar way, salinity-specific alkalinity can be defined as the ratio of alkalinity to salinity. By multiplying salinity-specific alkalinity with a constant salinity (S_{ref} , a S_{ref} value of 35 was used in this study), salinity-normalized alkalinity (NTA) has been widely used to adjust and compare TA data measured at different salinities [see Friis *et al.*, 2003, and references therein]:

$$NTA = TA * S_{ref} / S = slope * S_{ref} + TA_{S0} * S_{ref} / S \quad (3)$$

Assuming a well-defined oceanic end-member (S_{ocean} and TA_{ocean} , circle in Figure 2) and a linear relationship between TA and salinity, we elucidate the influences of SDC and non-SDC processes on TA_{S0} and NTA using

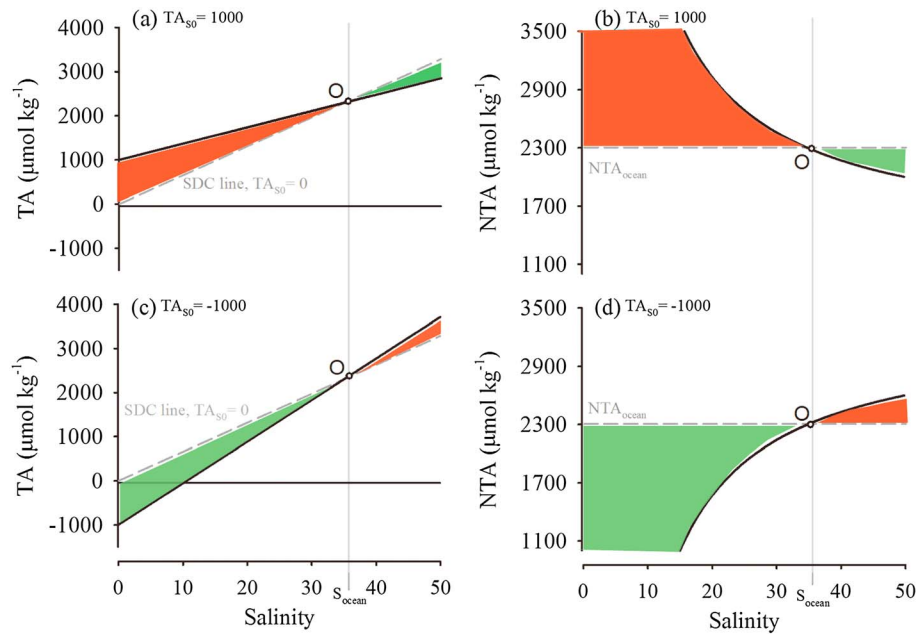


Figure 2. Schematic diagrams showing the influences of simple dilution or concentration (SDC) and non-SDC processes on TA-S plots. Here we assume a mean oceanic surface end-member O with $S_{\text{ocean}} = 35$, $TA_{\text{ocean}} = NTA_{\text{ocean}} = 2300 \mu\text{mol kg}^{-1}$. (a, b) We assume a positive y intercept (TA_{50}) of $1000 \mu\text{mol kg}^{-1}$, whereas (c, d) we assume a negative TA_{50} of $-1000 \mu\text{mol kg}^{-1}$. The dashed lines in panels Figures 2a and 2c show the TA-S changes due to the SDC effect, and those in Figures 2b and 2d refer to the NTA_{ocean} resulting from SDC processes. The effects of non-SDC additions and removals of TA are indicated by the orange- and green-shaded areas, respectively. As shown in Figures 2b and 2d, non-SDC TA addition results in values of NTA which are higher than NTA_{ocean} , while non-SDC removal lead to values of NTA which are lower than NTA_{ocean} .

the schematic diagrams in Figure 2. SDC processes (e.g., precipitation and evaporation) change TA along the line connecting the oceanic end-member and the zero-alkalinity freshwater end-member (referred to as the SDC line, Figures 2a and 2c). The addition or removal of zero-alkalinity freshwater results in a zero TA_{50} (Figures 2a and 2c) and a uniform NTA at all salinities (NTA_{ocean} in Figures 2b and 2d). In contrast, non-SDC changes in TA cause deviations in the TA-S relationship from the SDC line, while their effects on TA_{50} depends on the salinity at which they take place. A positive TA_{50} projection could be produced by non-SDC removal of TA at salinities higher than S_{ocean} (green-shaded area in Figure 2a) and/or non-SDC alkalinity addition at salinities lower than S_{ocean} (orange-shaded area in Figure 2a). Conversely, non-SDC TA addition at the high-salinity end (orange-shaded area in Figure 2c) and/or non-SDC TA removal at the low-salinity end (green-shaded area in Figure 2c) both result in a negative TA_{50} . At the same time that non-SDC processes lead to a nonzero TA_{50} , they also induce changes in NTA (Figures 2b and 2d). NTA now varies in proportion to the reciprocal of salinity (equation (3) and Figures 2b and 2d). For this reason, it was argued that this traditional normalization concept could cause an “overcorrection” and “artificial variance” by ignoring non-SDC processes [Friis et al., 2003]. Instead, a salinity normalization based on a constant and region-specific term for alkalinity of zero salinity was proposed by Friis et al. [2003]:

$$NTA_{eS} = (TA_{\text{obs}} - TA_{50}) * S_{\text{ref}}/S_{\text{obs}} + TA_{50} \quad (4)$$

where NTA_{eS} is the normalized alkalinity which accounts for the nonzero TA_{50} , and TA_{obs} and S_{obs} are the alkalinity and salinity from the observations. While the frequent occurrence of non-SDC processes rules out NTA as a universally appropriate salinity normalization technique [Friis et al., 2003], our analysis above suggests that NTA can be used as a useful indicator of the presence of non-SDC changes in alkalinity. At any salinity, non-SDC addition of TA causes a deviation of the TA-S relationship above the SDC line (Figure 2b) and an NTA higher than NTA_{ocean} (orange-shaded area in Figures 2b and 2d). Likewise, non-SDC removal of TA leads to an NTA lower than NTA_{ocean} at any salinity condition (green-shaded area in Figures 2b and 2d). These non-SDC changes can be attributed to non-SDC mixing (i.e., mixing with waters not on the SDC line) and/or biogeochemical processes.

Table 1. The Influences of Simple Dilution or Concentration (SDC) and Non-SDC Processes on TA, Salinity Normalized TA (NTA), and the y Intercept of the TA-S Relationship (TA_{S0}) Under Different Salinity Conditions^a

Controls		Effects			Example
Processes	Condition	TA-S	NTA	TA_{S0}	
SDC only	any salinity	on the SDC line	$NTA = NTA_{ocean}$	$TA_{S0} = 0$	Ocean gyres (precipitation/evaporation only) Mediterranean Sea in section 3.4
SDC + non-SDC addition	$S > S_{ocean}$	above the SDC line	$NTA > NTA_{ocean}$	$TA_{S0} < 0$	
SDC + non-SDC removal	$S < S_{ocean}$	below the SDC line	$NTA < NTA_{ocean}$	$TA_{S0} > 0$	The two ocean margins in section 3.3 Red Sea in section 3.4
	$S < S_{ocean}$			$TA_{S0} < 0$	

^aWe assume a well-defined oceanic end-member (S_{ocean} , TA_{ocean} , NTA_{ocean}); TA_{mix}^{SDC} is the alkalinity resulting from SDC mixing between the oceanic end-member and zero-alkalinity freshwater.

The influences of SDC and non-SDC processes on TA_{S0} and NTA are summarized in Table 1. In the following sections, these principles were used to investigate the observed TA-S relationship and TA_{S0} in a range of marine environments. For each region, NTA values were compared to the NTA_{ocean} to identify whether non-SDC TA changes are occurring, and further analysis was carried out to reveal the possible sources of any non-SDC changes.

3. Results

3.1. General Pattern

For all the SNOMS data, the measured TA varies strongly with salinity (Figure 3). Most open ocean data follows the SDC line through the global mean surface water end-member ($S = 35$, $TA = 2300 \mu\text{mol kg}^{-1}$). However, different slopes and intercepts of the TA-S relationships were observed in the Mediterranean Sea and the Red Sea (Figure 3). Deviations of TA from the SDC line are especially large at low salinities (Figure 3), which indicates the influences of riverine inputs, as well as biological and physical processes in coastal regions [Cai et al., 2010; Chen, 2002; Friis et al., 2003]. Accordingly, the results were divided into three geographic regimes: open ocean, ocean margins, and inland seas. The observational results are summarized in Table 2. A detailed examination of the variability in TA, the TA-S relationship, and NTA for each regime is presented below.

3.2. (Sub)Tropical Open Ocean

3.2.1. Atlantic

Previous work has shown that most of the TA variations in the Atlantic subtropical gyres (30°S–30°N) are associated with salinity changes, and the NTA is remarkably invariant [Millero et al., 1998]. Estimated from the CDIAC open ocean data (30°S–30°N, 70°W–20°E excluding the coastal regions, Figure S1a in the supporting

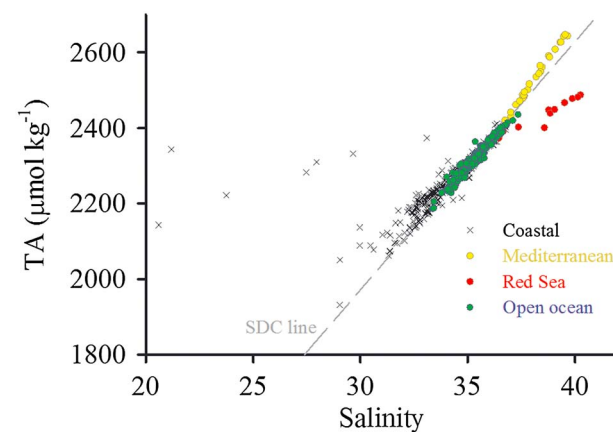


Figure 3. TA-S distributions in the open ocean, Mediterranean Sea, Red Sea, and coastal regions. All the SNOMS measurements ($n = 717$) are shown here. The dashed line shows the TA-S changes due to the simple dilution or concentration effect on the mean oceanic surface water ($S = 35$, $TA = 2300 \mu\text{mol kg}^{-1}$, an approximate average of the open ocean measurements).

information), the NTA_{ocean} of the (sub) tropical Atlantic is $2296 \pm 8 \mu\text{mol kg}^{-1}$ (mean ± 1 standard deviation, the same hereafter, $n = 1015$). It was also found that NTA in the Atlantic increases toward high latitudes due to intensified vertical mixing of TA-rich deep water [Millero et al., 1998]. SST is a potential proxy for the intensity of convective mixing and 20°C was used as the threshold to distinguish the high-latitude regime from the (sub)tropical regime [Lee et al., 2006; Millero et al., 1998]. For the SNOMS measurements, the NTA along the west-east North Atlantic transects (35°N–45°N, 60°W–0°W, Figure S1a) is $2292 \pm 4 \mu\text{mol kg}^{-1}$ ($n = 31$), which is not significantly different from that along the south-north Atlantic transect from Cape of Good Hope to North America ($2289 \pm 7 \mu\text{mol kg}^{-1}$, $n = 18$, Figure S1a). This suggests that TA additions from

Table 2. The Observations in the Surface Waters of Several Oceans and Seas by the SNOMS Project^a

(Sub)Tropics	Region	SST	Salinity	TA	NTA	NTA _{ocean} ^d
Open ocean	Atlantic ^b	22.23 ± 3.69	36.31 ± 0.35	2377 ± 22	2291 ± 5	2296 ± 8
	30°S–45°N, 70°W–20°E	16.20 to 28.40	35.57 to 37.34	2315 to 2436	2276 to 2302	
	Pacific ^c	26.76 ± 2.31	35.19 ± 0.61	2313 ± 40	2301 ± 9	2301 ± 10
	30°S–30°N, 180°W–140°W	19.43 to 30.48	33.36 to 36.58	2185 to 2404	2271 to 2341	
	Indian Ocean	24.93 ± 3.33	34.89 ± 0.55	2282 ± 37	2289 ± 6	2295 ± 7
	35°S–0°N, 20°E–100°E	16.51 to 28.99	34.19 to 35.66	2230 to 2336	2283 to 2304	
Ocean margins	western North Atlantic margin	17.28 ± 3.98	33.63 ± 0.85	2242 ± 45	2333 ± 15	2307 ± 5
	25°N–45°N, 155°W–115°W	9.85 to 25.69	31.25 to 35.43	2123 to 2336	2286 to 2378	
	eastern North Pacific margin	21.10 ± 7.97	34.19 ± 3.98	2319 ± 89	2426 ± 521	2290 ± 6
	20°N–45°N, 100°W–45°W	3.65 to 30.72	13.64 to 37.34	2051 to 2449	2279 to 6285	
Inland seas	Mediterranean Sea	21.84 ± 4.11	38.14 ± 0.88	2532 ± 73	2323 ± 15	2290 ± 4
	30°N–45°N, 7°W–40°E	15.28 to 27.68	36.74 to 39.65	2420 to 2647	2285 to 2344	
	Red Sea	29.15 ± 3.24	38.67 ± 1.33	2438 ± 40	2208 ± 44	2286 ± 9
	10°N–30°N, 30°E–45°E	22.85 to 32.76	36.43 to 40.24	2373 to 2488	2164 to 2284	

^aSea surface temperature (SST, °C), salinity, total alkalinity (TA), and the salinity-normalized alkalinity (NTA) are presented as “mean ± 1 standard deviation, minimum to maximum.” The concentrations of alkalinity are in units of $\mu\text{mol kg}^{-1}$. NTA is compared to that of the oceanic end-member (NTA_{ocean}).

^bExcluding the Mediterranean Sea.

^cExcluding the upwelling region in the eastern equatorial Pacific.

^dFor the open ocean, NTA was estimated from the CDIAC measurements in the defined region excluding the coastal data. For the ocean margins, NTA_{ocean} was estimated from the CDIAC measurements in the open ocean waters adjacent to the marginal systems under study. For the Mediterranean Sea and Red Sea, NTA_{ocean} was estimated from the CDIAC measurements in the inflowing water from the North Atlantic adjacent to the Strait of Gibraltar and that in the Arabian Sea adjacent to the Gulf of Aden, respectively. See the text for details.

deepwater convection are minor along these midlatitude North Atlantic transects, which is supported by the relatively warm SST observed (16.2 to 28.4°C). As a whole, the SNOMS measurements in the low-latitude and midlatitude Atlantic open ocean (30°S–45°N) showed a tight TA-S correlation ($R^2 = 0.94$, $n = 49$) and a relative constant NTA similar to the NTA_{ocean} estimated from CDIAC data (Figure S1d).

3.2.2. Pacific

In the subtropical Pacific gyres, *Millero et al.* [1998] reported a constant NTA of $2300 \pm 6 \mu\text{mol kg}^{-1}$. This is close to the NTA_{ocean} estimated from the CDIAC open ocean data adjacent to the SNOMS route ($2301 \pm 10 \mu\text{mol kg}^{-1}$, $n = 2245$, Figure S2a in the supporting information). In the eastern equatorial Pacific, higher NTA associated with the equatorial upwelling was observed with the NTA decreasing westward from the upwelling site [*Millero et al.*, 1998]. As the SNOMS sampling locations in the central equatorial Pacific were located far from the site of upwelling (Figure S2a), the influence of the equatorial upwelling is expected to be minor. For the SNOMS data in the (sub)tropical Pacific open ocean (30°S–30°N, 180°W–140°W excluding the upwelling region in the eastern equatorial Pacific, Figure S2a), we observed an NTA ($2301 \pm 9 \mu\text{mol kg}^{-1}$, $n = 195$) close to the NTA_{ocean} (Figure S2d).

3.2.3. Indian Ocean

There were only a few SNOMS measurements in the open ocean in the Indian Ocean (Figure 1). As shown in Table 1, the measurements show an NTA of $2289 \pm 6 \mu\text{mol kg}^{-1}$ ($n = 16$) which was not significantly different from the NTA_{ocean} of the Indian open ocean water estimated from the CDIAC data ($2295 \pm 7 \mu\text{mol kg}^{-1}$, $n = 420$).

Overall, the latitudinal distribution of the surface TA in the open ocean regime is similar to that of salinity (Figures S1 and S2), which is mainly determined by the rates of precipitation and evaporation at different latitudes [*Millero et al.*, 1998]. The SNOMS data in the (sub)tropical open oceans show a tight TA-S correlation along the SDC line (Figure 3) and relatively constant values of NTA which are similar to those of NTA_{ocean} (Table 2). This suggests that the TA variability in this region is mostly due to the SDC effects of precipitation and evaporation while non-SDC processes only play a minor role. The TA predicted from salinity and SST following *Lee et al.* [2006] generally agreed well with the measured alkalinity (not shown). The differences between the predicted values and the measurements ($0.3 \pm 10 \mu\text{mol kg}^{-1}$, $n = 304$) are similar to the estimated uncertainty of the prediction ($\pm 8.1 \mu\text{mol kg}^{-1}$ [*Lee et al.*, 2006]).

3.3. Ocean Margins

3.3.1. Western North Atlantic Margin

The TA distribution and TA-S relationship in the western North Atlantic margin have been extensively examined by *Cai et al.* [2010]. They identified a river-dominated two-end-member mixing type of TA-S relationship,

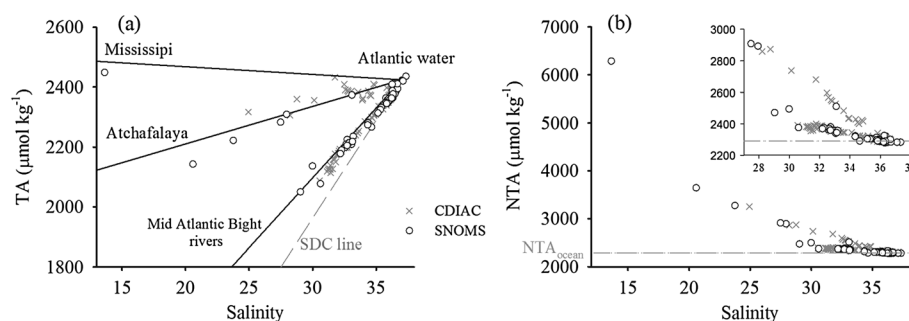


Figure 4. (a) TA-S and (b) salinity-normalized alkalinity (NTA)-S relationships in the western North Atlantic margin from the SNOMS and CDIAC data. (a) Adapted from Figure 2 by Cai *et al.* [2010]. The dashed SDC lines in Figures 4a and 4b show the TA-S and NTA-S changes due to simple dilution or concentration effects on the North Atlantic open ocean water. The solid lines in Figure 4a show the expected TA-S distributions assuming a two-end-member conservative mixing between the Atlantic water and the individual rivers. In Figure 4b, the NTA-S distribution at high salinities is highlighted in the inset.

as well as an alongshore current-dominated type which exhibits a segmented mixing line with a shared mid-salinity end-member [Cai *et al.*, 2010]. They also found that the intercepts of the TA-S regressions roughly match the concentrations of TA of the local rivers [Cai *et al.*, 2010]. We estimated the open ocean end-member for this region ($NTA_{\text{ocean}} = 2290 \pm 6 \mu\text{mol kg}^{-1}$, $n = 181$, Figure 4b) from the CDIAC measurements in the Atlantic water adjacent to the western North Atlantic margin ($25\text{--}40^\circ\text{N}$, $60\text{--}30^\circ\text{W}$, $S > 36$). During the SNOMS operation, samples were collected close to the U.S. East Coast and in the Gulf of Mexico (Figure 1). As shown in Figure 4, the SNOMS results agree well with those measured during the North American Carbon Program (NACP) U.S. East Coast cruise (obtained from CDIAC). Data at salinity values lower than 35 are above the SDC line (Figure 4a) with NTA higher than NTA_{ocean} (Figure 4b). The TA-S regression off the U.S. East Coast (Figure 4a) shows an intercept of $740 \mu\text{mol kg}^{-1}$ which is similar to the average concentration of the rivers entering the Mid-Atlantic Bight ($700 \mu\text{mol kg}^{-1}$) [Cai *et al.*, 2010]. The TA-S distribution in the Gulf of Mexico (Figure 4a) is also well constrained by the mixing lines of the oceanic end-member and the local rivers (Atchafalaya: $1960 \mu\text{mol kg}^{-1}$, Mississippi; $2375 \mu\text{mol kg}^{-1}$, data from Water Quality Data for the Nation (<http://waterdata.usgs.gov/nwis>) and Cai *et al.* [2010]). This river-dominated pattern shows that the mixing between river waters and seawater is the dominant controlling factor of the TA-S relationship in the western North Atlantic Ocean margin. The riverine non-SDC addition ($NTA > NTA_{\text{ocean}}$, Figure 4b) at the low-salinity end results in the positive values of TA_{50} that are close to TA concentrations of the local rivers (Figure 4a).

3.3.2. Eastern North Pacific Margin

As shown in Figure 5, the SNOMS and CDIAC data in the eastern North Pacific margin clearly show the influences of the low-salinity Columbia River plume off the coast of Oregon, the mid-salinity California Current that moves south along the western coast of North America [Batteen *et al.*, 1995; Schneider *et al.*, 2005], and the low-temperature and high-salinity coastal upwelling off northern California [Feely *et al.*, 2008]. As the Columbia River plume is separated from the open ocean water by the California Current, we observed a segmented TA-S mixing line with a shared California Current end-member at salinity ~ 32.5 (Figure 6a). This TA-S distribution shows a mixing between the river water and the California Current at $S < 32.5$, and a mixing between the California Current and the open ocean water at $S > 32.5$. The TA-S regression for the low-salinity data off the coast of Oregon ($S < 32.5$, Figure 6a) generates an intercept of $994 \pm 36 \mu\text{mol kg}^{-1}$ ($R^2 = 0.92$, $n = 77$), which agrees well with the TA concentration of the Columbia River ($1000 \mu\text{mol kg}^{-1}$) [Park, 1966, 1968; Park *et al.*, 1970].

The data measured in the eastern North Pacific margin generally falls above the SDC line (Figure 6a) with NTA higher than the NTA_{ocean} of the adjacent Pacific open ocean water ($120\text{--}45^\circ\text{N}$, $155\text{--}130^\circ\text{W}$, $S > 35$, $2307 \pm 5 \mu\text{mol kg}^{-1}$, $n = 69$). The non-SDC TA additions from the Columbia River and the California Current are clearly shown in the NTA distribution (Figure 5e) and the NTA-S relationship (Figure 6b). Moreover, coastal upwelling of “corrosive” water ($\Omega_{\text{aragonite}} < 1$) was observed off Northern California during the NACP U.S. West Coast cruise [Feely *et al.*, 2008]. As this upwelled water was undersaturated with respect to aragonite, the potential occurrence of dissolution of CaCO_3 may be an additional non-SDC source of surface alkalinity. In order to examine the importance of this biogeochemical effect, the results of the four NACP transects covering the Columbia River plume and the coastal upwelling (see the rectangle in Figure 5a) were highlighted in the

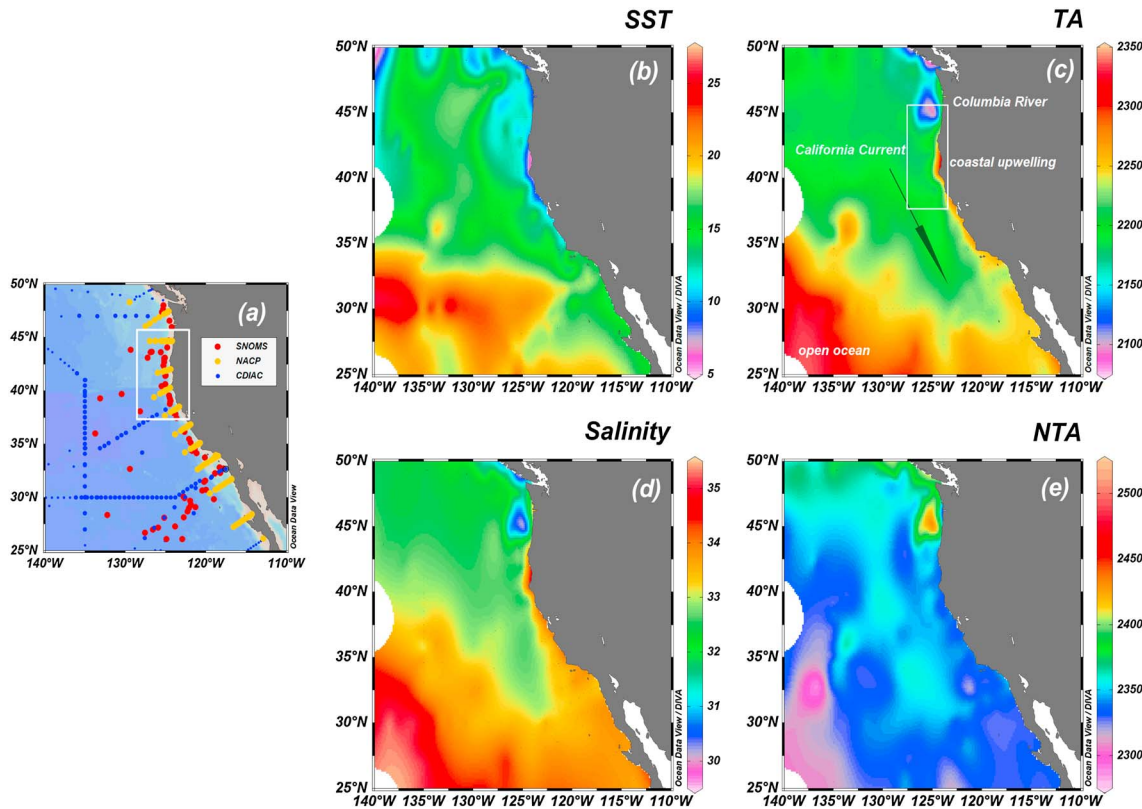


Figure 5. (a) Sampling positions of the SNOMS project in the western North Pacific margin and the CDIAC measurements in the same region including the NACP U.S. West Coast cruise 2007 [Feely and Sabine, 2011]; the sea surface distributions of (b) sea surface temperature (SST), (c) TA, (d) salinity, and (e) salinity-normalized alkalinity (NTA). The low-salinity water off Oregon is mainly from the Columbia River (Figure 5d); the coastal upwelling off northern California is indicated by the low SST (Figure 5b) and high salinity (Figure 5d). The NACP data in the white rectangle (Figure 5a) are highlighted in the inset to Figure 8b. Figure produced using Ocean Data View [Schlitzer, 2011].

inset to Figure 6b. It is shown that only a small increase in NTA was observed in the low-SST and high-salinity upwelled water, and this increase in NTA is much lower than that resulting from the Columbia river and the California current (Figure 6b).

3.4. Inland Seas

The Mediterranean Sea and the Red Sea are adjacent semiencllosed inland seas which are both located in arid regions. One notable feature for the two inland seas is that their TA-S variations are more significantly affected by evaporation than freshwater addition. As shown in Figure 7a and Table 2, the two inland seas are

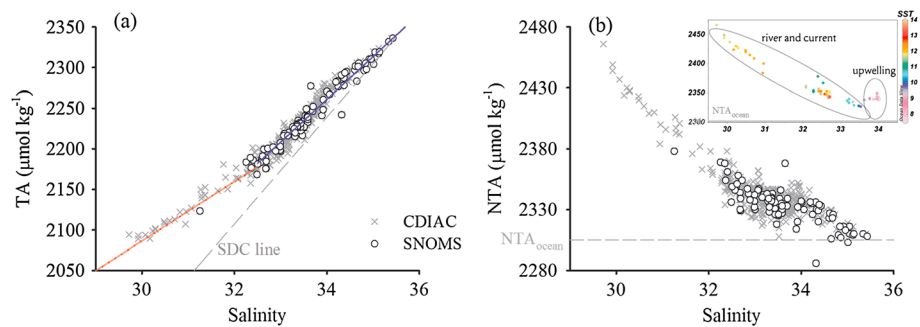


Figure 6. (a) TA-S and (b) salinity-normalized alkalinity (NTA)-S relationships in the eastern North Pacific margin from the SNOMS and the CDIAC data. In Figure 6a, the dashed SDC line shows the TA-S changes that would result from simple dilution or concentration of North Pacific open ocean water; the segmented TA-S mixing line shared a mid-salinity end-member at salinity ~ 32.5 . In Figure 6b, the dashed line is the NTA_{ocean} of the North Pacific open ocean water. The NACP measurements covering the river plume and coastal upwelling (within the white rectangle in Figure 7a) are highlighted in the inset to Figure 6b.

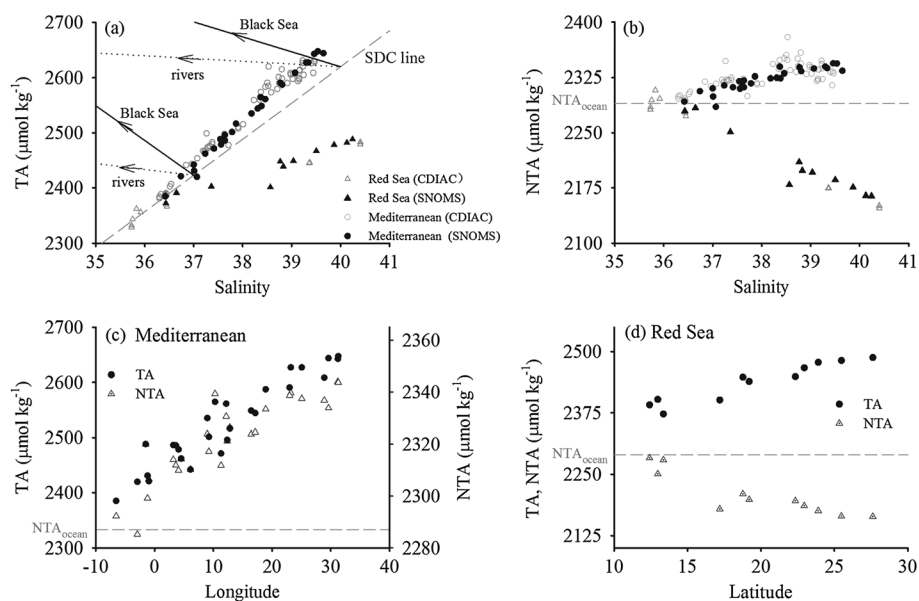


Figure 7. (a) TA-S and (b) salinity-normalized alkalinity (NTA)-S relationships in the Mediterranean Sea and the Red Sea from the SNOMS and CDIAC data; the distributions of TA and NTA against (c) longitude in the Mediterranean Sea and (d) latitude in the Red Sea. In Figure 7a, the dashed line shows the TA-S change due to the simple dilution or concentration effect on the mean open ocean water, and the arrow lines demonstrate TA-S variations in the Mediterranean Sea caused by mixing with alkaline waters from the local rivers and the Black Sea. In Figures 7b–7d, the dashed lines show the NTA_{ocean} of the inflowing waters from the North Atlantic into the Mediterranean Sea and from the Arabian Sea into the Red Sea, respectively.

both characterized by very high salinity and TA. Despite the similar salinity range (36.4 to 40.2, Figure 7a), the concentrations of TA in the Mediterranean Sea (2420 to $2647 \mu\text{mol kg}^{-1}$) are much higher than those in the Red Sea (2373 to $2488 \mu\text{mol kg}^{-1}$). The TA-S relationships in the two seas deviate from the SDC line in different directions (Figure 7a), and the NTA clearly suggests different non-SDC processes (Figure 7b): one adding TA to the Mediterranean Sea ($NTA > NTA_{ocean}$), and the other removing TA from the Red Sea ($NTA < NTA_{ocean}$).

3.4.1. Mediterranean Sea

The Mediterranean Sea is characterized by an antiestuarine thermohaline circulation resulting from a negative freshwater balance [Lascazatos *et al.*, 1999]. The surface water in the Mediterranean Sea is from the inflowing Atlantic water through the Strait of Gibraltar [Lascazatos *et al.*, 1999]. We thus used the Atlantic water adjacent to the Strait of Gibraltar as the ocean end-member ($NTA_{ocean} = 2290 \pm 4 \mu\text{mol kg}^{-1}$, $n = 49$). In the Mediterranean Sea, salinity and TA increase eastward away from the Atlantic inflow due to evaporation (Figure 7c). The NTA also increases eastward (Figure 7c), and the high NTA ($NTA > NTA_{ocean}$) suggests additional TA sources due to non-SDC processes. This can be explained by the alkalinity inputs from the local rivers: the Rhone, Po, Nile, Ebro, Tiber, and Adige ($S = 0$, discharge-weighted $TA = 2820 \mu\text{mol kg}^{-1}$) and from the Black Sea and Sea of Marmara ($S = 29.3$, $TA = 2909 \mu\text{mol kg}^{-1}$) [Schneider *et al.*, 2007]. Although the coral reefs in the Mediterranean Sea [Aguilar, 2007] may result in calcification-induced decreases in TA, this TA sink ($0.4 \times 10^{12} \text{ mol yr}^{-1}$ [Copin-Montégut, 1993]) is much smaller than the TA influx from rivers and the Black Sea ($2.7 \times 10^{12} \text{ mol yr}^{-1}$ [Schneider *et al.*, 2007]).

The TA and salinity in the Mediterranean Sea show a good correlation ($TA = 79.84 * S - 510$, $R^2 = 0.97$, $n = 92$, Figure 7a), but the negative intercept does not represent the local riverine input. Negative TA_{S0} was also observed at the Dyfamed site in the northwest Mediterranean Sea by Copin-Montégut and Bégovic [2002] ($-1038 \mu\text{mol kg}^{-1}$), and along a west-east transection in the Mediterranean Sea by Schneider *et al.* [2007] ($-682 \mu\text{mol kg}^{-1}$). This phenomenon is caused by the exceptional Mediterranean environment: the non-SDC alkalinity additions from the local rivers and the Black Sea mainly occur in the eastern Mediterranean where salinity is higher than S_{ocean} (strong evaporation). As demonstrated in Figure 2c, the non-SDC addition of TA at the high salinity end ($S > S_{ocean}$) results in a steeper TA-S slope than the SDC line, and in a negative TA_{S0} .

3.4.2. Red Sea

The Red Sea lies between the Mediterranean Sea and the Indian Ocean. It is a deep trench resulting from the separation of the Arabian plate from the African plate [Bosworth *et al.*, 2005]. The water circulation pattern in the Red Sea is similar to that in the Mediterranean Sea. The major source of the surface water in the Red Sea is the inflowing water from the Arabian Sea through the Gulf of Aden ($\text{NTA}_{\text{ocean}} = 2289 \pm 9 \mu\text{mol kg}^{-1}$, $n = 22$). Due to evaporation during the northward advection of the surface water, the salinity and TA in the northern Red Sea are higher than those in the southern part (Figure 7d). In contrast, NTA decreases northward to concentrations lower than $\text{NTA}_{\text{ocean}}$ (Figure 7d) indicating non-SDC alkalinity removal in the Red Sea.

The Red Sea is a simpler system for examining the alkalinity cycling because there are no major rivers entering it. We therefore attributed the non-SDC alkalinity removal solely to biogeochemical processes. Coral reefs are widely distributed in the Red Sea, and the coral diversity is considered among the highest in the India Ocean region [PERSGA, 2000, 2010]. The surface water in the Red Sea is oversaturated with respect to CaCO_3 ($\Omega_{\text{aragonite}} = 4.08 \pm 0.26$, $n = 22$) which may promote the biological formation of calcareous shells and skeletons. Ellis and Milliman [1985] suggested that the suspended CaCO_3 particles in the Red Sea are either biogenic or detrital rather than formed by inorganic precipitation. Because of the biogenic precipitation of CaCO_3 and the sinking of surface water due to the high evaporation, depth profiles of salinity-specific alkalinity in the Red Sea showed lower values compared to those in the adjacent Gulf of Aden [Anderson and Dyrssen, 1994]. As undersaturation of CaCO_3 is never reached in the whole water column of the Red Sea [Elageed, 2010], the sedimentation and accumulation of CaCO_3 is favored, and deep-sea carbonate sediments are found in the Red Sea [Al-Fukaha, 1994; Al-Rousan, 1998; Gevirtz and Friedman, 1966]. The Red Sea is estimated to be a sink for TA of $1.65 \times 10^{12} \text{ mol yr}^{-1}$ [Anderson and Dyrssen, 1994]. As discussed above, the loss of TA in the Red Sea is mainly due to biogenic calcification and CaCO_3 sedimentation. This non-SDC TA removal at the high-salinity end results in a positive intercept even though there is no significant freshwater influx to the Red Sea.

4. Discussions

The oceanic uptake of anthropogenic CO_2 has no direct effect on alkalinity, and even if ocean acidification eventually causes an indirect increase in surface alkalinity because of reduced calcification, such a change will not be detectable for at least several decades [Ilyina *et al.*, 2009]. It has been shown that the surface TA in the world's major oceans can be estimated from salinity and SST with a reasonable accuracy [Lee *et al.*, 2006]. When combining TA with the existing pCO_2 observations, the whole carbonate system in the surface ocean can be characterized [Millero *et al.*, 1998]. As the global fields of SST (<http://www.ospo.noaa.gov/Products/ocean/sst.html>) and salinity (<http://aquarius.nasa.gov/>) are now available from remote sensing, it is possible to use satellite data to improve studies of the global distribution and variability of TA, although the accuracy of such an approach has yet to be established.

However, no global empirical algorithms can be developed for coastal regions due to the complex physical and biological interactions in these dynamic environments. For instance, under the influences of various rivers, different concentrations of TA can be observed at the same salinity in the western North Atlantic margin (Figure 4a). It is also difficult for the algorithms to account for non-SDC biological changes in TA, particularly during episodic blooms of coccolithophores. Moreover, phytoplankton and bacterial cells [Kim *et al.*, 2006] and chemically reactive particles [Sejr *et al.*, 2011] could affect TA measurements, while organic bases could contribute to alkalinity in biologically productive waters or waters with high organic loads [Cai *et al.*, 1998; Hernandez-Ayon *et al.*, 2007; Jiang *et al.*, 2014; Kim and Lee, 2009; Muller and Bleie, 2008]. These biogeochemical effects are usually minor in the open ocean but can be significant in coastal waters, which are more biogeochemically active. The concept of potential alkalinity [Brewer *et al.*, 1975], which corrects for the alkalinity changes resulting from nutrient uptake and release, can be useful in allowing the processes involving CaCO_3 to be more easily quantified. We have demonstrated that TA_{50} can either be positive or negative depending on the non-SDC changes in TA at different salinities (Figure 2 and Table 1). As a result, the river end-member can only be reliably estimated from TA_{50} when river input dominates as the only significant mechanism controlling the TA-S relationship (e.g., in estuaries and river plumes).

Figure 2 and Table 1 assume a simple two-end-member linear mixing. However, the mixing processes in the ocean often consist of more than two end-members. Taking coastal systems with multiple river inputs and a

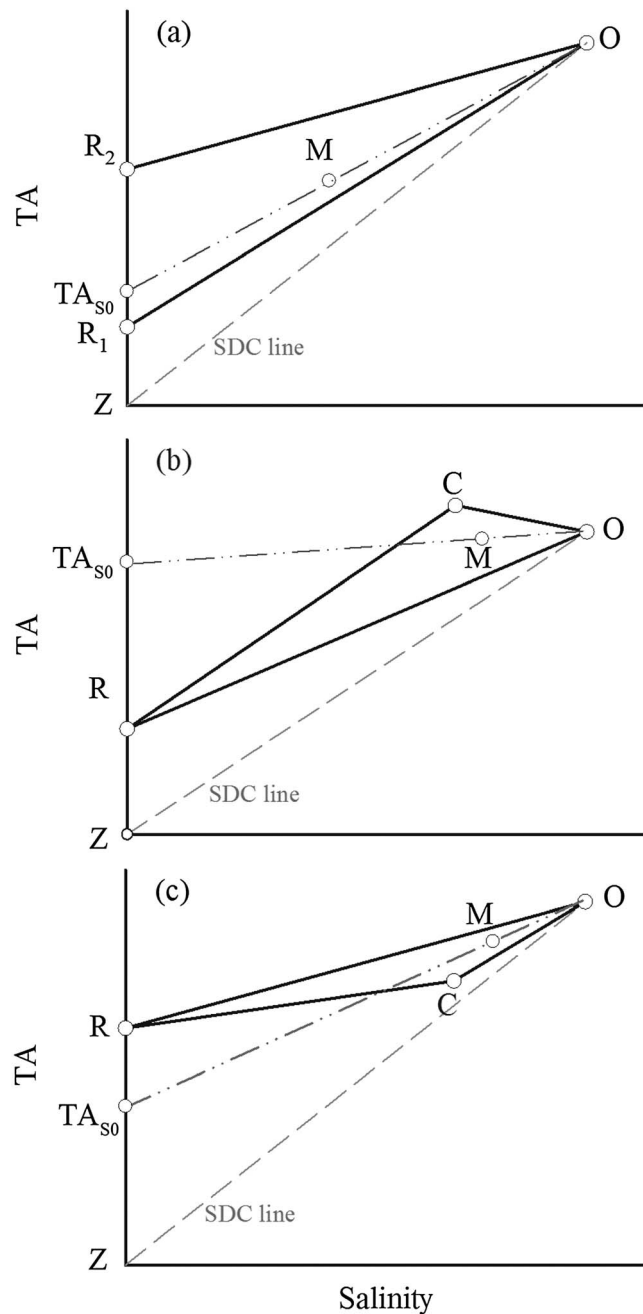


Figure 8. Schematic of the TA-S relationship in coastal systems with (a) two river end-members R_1 and R_2 ; (b, c) one river end-member R and one shelf current end-member C with different concentrations of TA. Adapted from *Cai et al.* [2010]. The points Z and O refer to the end-members of zero-alkalinity freshwater and oceanic water, respectively. The dashed SDC lines show the TA-S changes due to the simple dilution or concentration effect on the oceanic water. We assume that the TA-S regression line goes through the oceanic end-member and the mixture (M) generating an intercept at TA_{S0} . See the text for details.

line OR , TA_{S0} would be higher than TA_R (Figure 8b), and vice versa (Figure 8c). In the western North Atlantic margin, the segmented TA-S mixing line observed by *Cai et al.* [2010] was not clearly seen in our study (Figure 4a). This is probably due to the lack of data points at low salinities. However, the reasonably good

shelf current as an example (Figure 8), we discuss how mixing schemes with multiple end-members affect TA_{S0} . It should be noted that our discussion here focuses only on the physical aspect and does not take into account the biogeochemical effect (i.e., assuming $\Delta TA_{bgc} = 0$ in equation (1)). In Figure 8a, we consider a simple system with two river end-members R_1 and R_2 ($TA_{R2} > TA_{R1}$); Z and O refer to the end-members of the zero-alkalinity freshwater and the open ocean water, respectively. In most estuaries, salinity and TA changes due to SDC processes can be safely ignored when compared to riverine inputs. As a result, the mixture (M in Figure 8a) must fall within the range constrained by the triangle R_1R_2O while its exact position within the triangle depends on the contributions of the different end-members. If river R_1 is the more dominant contributor to the mixing (e.g., near the estuary of river R_1), the data will be closer to the line OR_1 and the TA-S regression will give an intercept closer to TA_{R1} . If R_1 and R_2 are well mixed before they mix with seawater (e.g., R_1 and R_2 are tributaries of a big river), the TA_{S0} at zero salinity will be a flow-weighted mean concentration of the two rivers.

In Figures 8b and 8c, we add a shelf current end-member (C) in addition to the integrated river end-member (R). As shown by our observations in the eastern North Pacific margin (Figure 6a), the current-dominated type of mixing shows a segmented TA-S line with a shared shelf current end-member at mid-salinity [*Cai et al.*, 2010], i.e., lines RC and CO in Figures 8b and 8c. If the mixture (M) consists of waters from the three end-members, M will fall in the triangle RCO (Figure 8). The difference between TA_{S0} and the river water concentration (TA_R) depends on the deviation of the current end-member from the mixing line of the oceanic water and the river water (line OR in Figures 8b and 8c). If C is above the

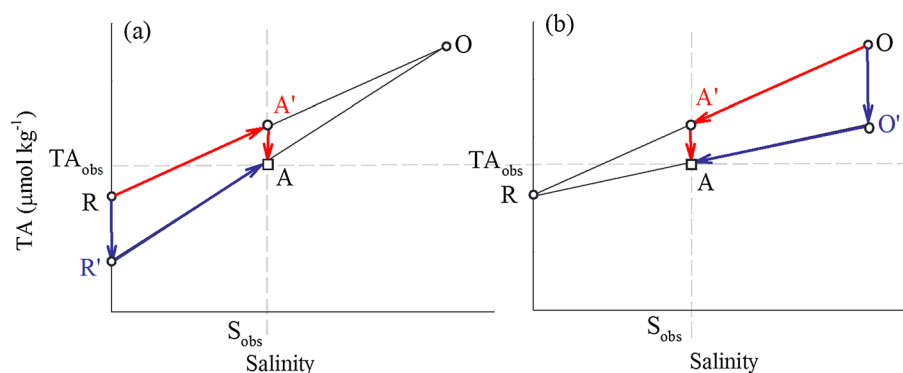


Figure 9. Schematic diagrams showing alternative explanation of how the combined effect of mixing and biogeochemical can produce an observed point A which deviates from the conservative mixing line between the two end-members (R and O). The trajectory of alkalinity change follows (a) RR'A or (b) OO'A if biogeochemical change precedes mixing; or alternatively RA'A in Figure 9a or OA'A in Figure 9b if biogeochemical change takes place after mixing. See the text for details.

agreement between the values of TA_{S_0} and the river TA concentrations (Figure 4a) suggests that the shelf current end-member should not lie far from the river–oceanic water mixing line.

It should be noted that when mixing and biogeochemical impacts are both involved then the summed effect will depend on the order in which the processes occur, as shown in Figure 9. Point A corresponds to an observed value of TA at an intermediate salinity where A is not on the mixing line between the freshwater end-member R and the oceanic end-member O. The interpretation of the combination of mixing and biogeochemical processes that leads to point A depends on the order in which they are considered to have taken place. When the biogeochemical change precedes mixing, the end-member property changes before the conservative mixing (the trajectory of alkalinity change proceeds from R to R' to A in Figure 9a or O to O' to A in Figure 9b). On the other hand, if the biogeochemical change takes place after mixing, this implies a trajectory from R to O to A' to A in Figure 9a or O to A' to A in Figure 9b. The calculated biogeochemical changes (RR', OO', or AA' in Figure 9) are rather different depending on the assumed order.

5. Conclusions

The SNOMS project provided surface measurements across a large and diverse range of (sub)tropical marine environments. In order to better study the variability of TA, we developed a generally applicable theoretical framework (as summarized in Figure 2 and Table 1) which elucidates how TA and NTA respond to simple dilution or concentration (SDC) and non-SDC processes. In the low-latitude and midlatitude open ocean waters of the Atlantic, Pacific (excluding the equatorial upwelling), and Indian Oceans, TA-S distributions generally followed the SDC line and relatively constant values of NTA were observed (Table 2). In other words, the TA variability in these oligotrophic surface waters is mostly controlled by the SDC effects of precipitation and evaporation. In ocean margins and inland seas, deviations of the TA-S relationship from the SDC line indicate the occurrences of non-SDC processes. Using NTA as an indicator, the non-SDC additions (producing $NTA > NTA_{ocean}$) and removals (producing $NTA < NTA_{ocean}$) of alkalinity can be identified. The non-SDC TA additions in the western North Atlantic margin and eastern North Pacific margin are caused by inflow of rivers and shelf currents, and the high NTA ($>NTA_{ocean}$) in the Mediterranean Sea is attributed to alkalinity inputs from local rivers and the Black Sea. Conversely, the low NTA ($NTA < NTA_{ocean}$) results from TA removal into newly formed (and subsequently exported) $CaCO_3$. In river-dominated marginal systems, the non-SDC TA addition at $S < S_{ocean}$ lead to positive values of TA_{S_0} which are close to the TA concentrations of the local rivers. In contrast, the non-SDC TA addition in the Mediterranean Sea and the non-SDC TA removal in the Red Sea, both occurring at $S > S_{ocean}$, result in negative and positive TA_{S_0} , respectively.

Our analyses of these diverse systems lead to several recommendations. When TA_{S_0} is not zero, NTA shows a nonlinear relationship with salinity and can exhibit large deviations from NTA_{ocean} that are not necessarily caused by biogeochemical processes (Figures 2b and 2d). This is the reason that NTA is not a universally appropriate salinity normalization method, and why it is important that the nonzero TA_{S_0} should be included in the normalization [Friis *et al.*, 2003]. However, NTA was found to be a useful indicator of the activity of

non-SDC processes (Figure 2 and Table 1). The non-SDC changes in alkalinity generate either positive or negative TA_{50} depending on the salinities at which they take place (Figure 2 and Table 1). In coastal regions, our study suggests that estimating the river water TA concentration from TA_{50} is likely to be successful only in river-dominated systems. In contrast, where there are large impacts from other physical (e.g., evaporation, shelf currents, and upwelling) and biological processes (e.g., calcification, uptake, and release of nutrients), they act to decouple TA_{50} from the river water concentration.

Acknowledgments

The Swire Charitable Trust is gratefully acknowledged for funding the SNOMS project, and the Swire Group Company China Navigation is thanked for providing access to the M/V *Pacific Celebes*. The Swire Education Trust is acknowledged for providing the scholarship for Zong-Pei Jiang's PhD study. This work would not have been possible without the help of the ship's crews and support staff on shore—particularly the engine room staff during their daily sample collections. We thank all the people at NOCS who have supported the development, operation, sample analysis, and data processing of the SNOMS project, and we name here only a few of them—Mark Hartman, Jon Campbell, Dave Childs, and Maureen Pagnani. Constructive comments from Andrew Dickson, Dieter Wolf-Gladrow, and another anonymous reviewer significantly improved the quality of this paper. We are grateful to Andrew Dickson for pointing out the importance of the order in which mixing and biogeochemical impacts take place.

References

- Abril, G., H. Etcheber, B. DeLille, M. Frankignoulle, and A. V. Borges (2003), Carbonate dissolution in the turbid and eutrophic Loire estuary, *Mar. Ecol. Prog. Ser.*, **259**, 129–138, doi:10.3354/meps259129.
- Aguilar, R. (2007), *The Corals of the Mediterranean*, 83 pp., Oceana, Fondazione Zegna, Biella, Italy.
- Al-Fukaha, F. (1994), A textural and geochemical study on reefal sediments of the Gulf of Aqaba, and the input of airborne dust to the area, MS thesis, Yarmouk Univ., Irbid, Jordan.
- Al-Rousan, S. (1998), Sediment role in nutrient cycle within coral reefs of the Gulf of Aqaba, Red Sea, MS thesis, Yarmouk Univ., Irbid, Jordan.
- Anderson, L., and D. Dyrssen (1994), Alkalinity and total carbonate in the Arabian Sea. Carbonate depletion in the Red Sea and Persian Gulf, *Mar. Chem.*, **47**(3–4), 195–202, doi:10.1016/0304-4203(94)90019-1.
- Bates, N. R., A. F. Michaels, and A. H. Knap (1996), Alkalinity changes in the Sargasso Sea: Geochemical evidence of calcification?, *Mar. Chem.*, **51**(4), 347–358.
- Batteen, M. L., C. A. Collins, C. R. Gunderson, and C. S. Nelson (1995), The effect of salinity on density in the California Current system, *J. Geophys. Res.*, **100**(C5), 8733–8749, doi:10.1029/95JC00424.
- Bosworth, W., P. Huchon, and K. McClay (2005), The Red Sea and Gulf of Aden basins, *J. Afr. Earth Sci.*, **43**(1–3), 334–378.
- Brewer, P. G., and J. C. Goldman (1976), Alkalinity changes generated by phytoplankton growth, *Limnol. Oceanogr.*, **21**(1), 108–117.
- Brewer, P. G., G. T. F. Wong, M. P. Bacon, and D. W. Spencer (1975), An oceanic calcium problem?, *Earth Planet. Sci. Lett.*, **26**(1), 81–87.
- Cai, W. J., Y. C. Wang, and R. E. Hodson (1998), Acid-base properties of dissolved organic matter in the estuarine waters of Georgia, USA, *Geochim. Cosmochim. Acta*, **62**(3), 473–483, doi:10.1016/S0016-7037(97)00363-3.
- Cai, W. J., X. P. Hu, W. J. Huang, L. Q. Jiang, Y. C. Wang, T. H. Peng, and X. Zhang (2010), Alkalinity distribution in the western North Atlantic Ocean margins, *J. Geophys. Res.*, **115**, C08014, doi:10.1029/2009JC005482.
- Cao, Z. M., M. H. Dai, N. Zheng, D. L. Wang, Q. Li, W. D. Zhai, F. F. Meng, and J. P. Gan (2011), Dynamics of the carbonate system in a large continental shelf system under the influence of both a river plume and coastal upwelling, *J. Geophys. Res.*, **116**, G02010, doi:10.1029/2010JG001596.
- Chen, C.-T. A. (2002), Shelf-vs. dissolution-generated alkalinity above the chemical lysocline, *Deep Sea Res., Part II*, **49**(24–25), 5365–5375, doi:10.1016/S0967-0645(02)00196-0.
- Copin-Montégut, C. (1993), Alkalinity and carbon budgets in the Mediterranean Sea, *Global Biogeochem. Cycles*, **7**(4), 915–925, doi:10.1029/93GB01826.
- Copin-Montégut, C., and M. Bégovic (2002), Distributions of carbonate properties and oxygen along the water column (0–2000 m) in the central part of the NW Mediterranean Sea (Dyfamed site): Influence of winter vertical mixing on air-sea CO_2 and O_2 exchanges, *Deep Sea Res., Part II*, **49**(11), 2049–2066, doi:10.1016/S0967-0645(02)00027-9.
- Dickson, A. G. (1981), An exact definition of total alkalinity and a procedure for the estimation of alkalinity and total inorganic carbon from titration data, *Deep Sea Res., Part I*, **28**(6), 609–623, doi:10.1016/0198-0149(81)90121-7.
- Dickson, A. G. (1992), The development of the alkalinity concept in marine chemistry, *Mar. Chem.*, **40**(1–2), 49–63.
- Dickson, A. G., C. L. Sabine, and J. R. Christian (2007), *Guide to Best Practices for Ocean CO_2 Measurements*, 191 pp., North Pacific Marine Science Organization (PICES), Sidney, B. C., Canada.
- Doney, S. C. (2009), The consequences of human-driven ocean acidification for marine life, F1000 Biol Rep., 36 pp., Department of Marine Chemistry and Geochemistry, Woods Hole Oceanographic Institution, Woods Hole, Mass.
- Doney, S. C., V. J. Fabry, R. A. Feely, and J. A. Kleypas (2009), Ocean acidification: The other CO_2 problem, *Annu. Rev. Mar. Sci.*, **1**, 169–192.
- Elageed, S. (2010), Factors controlling the total alkalinity in the Arabian Sea and Red Sea, MS thesis, Univ. of Bergen, Bergen, Norway.
- Ellis, J. P., and J. D. Milliman (1985), Calcium-carbonate suspended in Arabian Gulf and Red-Sea waters—Biogenic and detrital, not chemogenic, *J. Sediment. Petrol.*, **55**(6), 805–808.
- Feely, R. A., and C. Sabine (2011), Carbon dioxide and hydrographic measurements during the 2007 NACP West Coast cruise, Carbon Dioxide Information Analysis Center, Oak Ridge Natl. Lab., U. S. Department of Energy, Oak Ridge, Tenn., doi:10.3334/CDIAC/otg.CLIVAR_NACP_West_Coast_Cruise_2007. [Available at http://cdiac.ornl.gov/ftp/oceans/NACP_West_Coast_Cruise_2007/]
- Feely, R. A., C. L. Sabine, K. Lee, W. Berelson, J. Kleypas, V. J. Fabry, and F. J. Millero (2004), Impact of anthropogenic CO_2 on the $CaCO_3$ system in the oceans, *Science*, **305**(5682), 362–366, doi:10.1126/science.1097329.
- Feely, R. A., C. L. Sabine, J. M. Hernandez-Ayon, D. Janson, and B. Hales (2008), Evidence for upwelling of corrosive “acidified” water onto the continental shelf, *Science*, **320**(5882), 1490–1492, doi:10.1126/science.1155676.
- Friis, K., A. Körtzinger, and D. W. R. Wallace (2003), The salinity normalization of marine inorganic carbon chemistry data, *Geophys. Res. Lett.*, **30**(2), 1085, doi:10.1029/2002GL015898.
- Gevirtz, J. L., and G. M. Friedman (1966), Deep-sea carbonate sediments of the Red Sea and their implications on marine lithification, *J. Sediment. Petrol.*, **36**(1), 143–151.
- Harlay, J., et al. (2010), Biogeochemical study of a coccolithophore bloom in the northern Bay of Biscay (NE Atlantic Ocean) in June 2004, *Prog. Oceanogr.*, **86**, 317–336.
- Harlay, J., et al. (2011), Biogeochemistry and carbon mass balance of a coccolithophore bloom in the northern Bay of Biscay (June 2006), *Deep Sea Res., Part I*, **58**(2), 111–127.
- Hernandez-Ayon, J. M., A. Zirino, A. G. Dickson, T. Camiro-Vargas, and E. Valenzuela-Espinoza (2007), Estimating the contribution of organic bases from microalgae to the titration alkalinity in coastal seawaters, *Limnol. Oceanogr. Methods*, **5**, 225–232.
- Hydes, D. J., Z. Jiang, M. C. Hartman, J. M. Campbell, S. E. Hartman, M. R. Pagnani, B. A. Kelly-Gerrey, and T. Tyrrell (2012), Surface DIC and TALK measurements along the M/V Pacific Celebes VOS Line during the 2007–2012 cruises, Carbon Dioxide Information Analysis Center, Oak Ridge Natl. Lab., U. S. Department of Energy, Oak Ridge, Tenn., doi:10.3334/CDIAC/OTG.VOS_PC_2007-2012. [Available at http://cdiac.ornl.gov/ftp/oceans/VOS_Pacific_Celebes_line/]

- Hydes, D. J., M. C. Hartman, J. M. Campbell, Z.-P. Jiang, S. E. Hartman, M. Pagnani, B. A. Kelly-Gerrey, and J. Donahoe (2013), *Report of the SNOMS Project 2006 to 2012, SNOMS: SWIRE NOCS Ocean Monitoring System. Part 1: Narrative Description*, Report 33, National Oceanography Centre Research and Consultancy, Southampton, U. K.
- Ilyina, T., R. E. Zeebe, E. Maier-Reimer, and C. Heinze (2009), Early detection of ocean acidification effects on marine calcification, *Global Biogeochem. Cycles*, 23, GB1008, doi:10.1029/2008GB003278.
- Jiang, Z.-P., et al. (2014), Application and assessment of a membrane-based pCO₂ sensor under field and laboratory conditions, *Limnol. Oceanogr. Methods*, 12, 262–278.
- Key, R. M., A. Kozyr, C. L. Sabine, K. Lee, R. Wanninkhof, J. L. Bullister, R. A. Feely, F. J. Millero, C. Mordy, and T. H. Peng (2004), A global ocean carbon climatology: Results from Global Data Analysis Project (GLODAP), *Global Biogeochem. Cycles*, 18, GB4031, doi:10.1029/2004GB002247.
- Kim, H.-C., and K. Lee (2009), Significant contribution of dissolved organic matter to seawater alkalinity, *Geophys. Res. Lett.*, 36, L20603, doi:10.1029/2009GL040271.
- Kim, H.-C., K. Lee, and W. Y. Choi (2006), Contribution of phytoplankton and bacterial cells to the measured alkalinity of seawater, *Limnol. Oceanogr.*, 51(1), 331–338.
- Koczy, F. F. (1956), The specific alkalinity, *Deep Sea Res.*, 3(4), 279–288.
- Lascaratos, A., W. Roether, K. Nittis, and B. Klein (1999), Recent changes in deep water formation and spreading in the eastern Mediterranean Sea: A review, *Prog. Oceanogr.*, 44(1–3), 5–36, doi:10.1016/S0079-6611(99)00019-1.
- Lee, K., L. T. Tong, F. J. Millero, C. L. Sabine, A. G. Dickson, C. Goyet, G. H. Park, R. Wanninkhof, R. A. Feely, and R. M. Key (2006), Global relationships of total alkalinity with salinity and temperature in surface waters of the world's oceans, *Geophys. Res. Lett.*, 33, L19605, doi:10.1029/2006GL027207.
- Liu, Q., M. Dai, W. Chen, C. A. Huh, G. Wang, Q. Li, and M. A. Charette (2012), How significant is submarine groundwater discharge and its associated dissolved inorganic carbon in a river-dominated shelf system?, *Biogeosciences*, 9(5), 1777–1795, doi:10.5194/bg-9-1777-2012.
- Millero, F. J., K. Lee, and M. Roche (1998), Distribution of alkalinity in the surface waters of the major oceans, *Mar. Chem.*, 60(1–2), 111–130.
- Muller, F. L. L., and B. Bleie (2008), Estimating the organic acid contribution to coastal seawater alkalinity by potentiometric titrations in a closed cell, *Anal. Chim. Acta*, 619(2), 183–191, doi:10.1016/j.aca.2008.05.018.
- Orr, J. C., et al. (2005), Anthropogenic ocean acidification over the twenty-first century and its impact on calcifying organisms, *Nature*, 437(7059), 681–686, doi:10.1038/Nature04095.
- Park, K. (1968), Alkalinity and pH off the coast of Oregon, *Deep Sea Res.*, 15(2), 171–183.
- Park, P. K. (1966), Columbia River plume identification by specific alkalinity, *Limnol. Oceanogr.*, 11, 118–120.
- Park, P. K., G. R. Webster, and R. Yamamoto (1970), *Alkalinity Budget of the Columbia River*, Department of Oceanography, Oregon State Univ., Corvallis, Ore.
- PERSGA (2000), *Coral reefs in the Red Sea and Gulf of Aden Surveys 1990 to 2000 Summary and Recommendations*, PERSGA Technical Series No. 7, The Regional Organization for the Conservation of the Environment of the Red Sea and Gulf of Aden, Jeddah, Saudi Arabia.
- PERSGA (2010), *The Status of Coral Reefs in the Red Sea and Gulf of Aden: 2009*, PERSGA Technical Series No. 16, The Regional Organization for the Conservation of the Environment of the Red Sea and Gulf of Aden, Jeddah, Saudi Arabia.
- Sarmiento, J. L., and N. Gruber (2006), *Ocean Biogeochemical Dynamics*, 528 pp., Princeton Univ. Press, Princeton, N. J.
- Sarmiento, J. L., J. Dunne, A. Gnanadesikan, R. M. Key, K. Matsumoto, and R. Slater (2002), A new estimate of the CaCO₃ to organic carbon export ratio, *Global Biogeochem. Cycles*, 16(4), 1107, doi:10.1029/2002GB001919.
- Schlitzer, R. (2011), Ocean data view. [Available at <http://odv.awi.de/>]
- Schneider, A., D. W. R. Wallace, and A. Körtzinger (2007), Alkalinity of the Mediterranean Sea, *Geophys. Res. Lett.*, 34, L15608, doi:10.1029/2006GL028842.
- Schneider, B., and W. Roether (2007), Meteor 06MT20011018 cruise data from the 2001 cruises, CARINA data set, Carbon Dioxide Information Analysis Center, Oak Ridge Natl. Lab., U. S. Department of Energy, Oak Ridge, Tenn., doi:10.3334/CDIAC/otg.CARINA_06MT20011018. [Available at <http://cdiac.ornl.gov/ftp/oceans/CARINA/Meteor/06MT512/>]
- Schneider, N., E. Di Lorenzo, and P. P. Niiler (2005), Salinity variations in the Southern California Current, *J. Phys. Oceanogr.*, 35(8), 1421–1436.
- Sejr, M. K., D. Krause-Jensen, S. Rysgaard, L. L. Sorensen, P. B. Christensen, and R. N. Glud (2011), Air-sea flux of CO₂ in Arctic coastal waters influenced by glacial melt water and sea ice, *Tellus, Ser. B*, 63(5), 815–822.
- Suzuki, T., et al. (2013), PACIFICA data synthesis project, ORNL/CDIAC-159, NDP-092, Carbon Dioxide Information Analysis Center, Oak Ridge Natl. Lab., U. S. Department of Energy, Oak Ridge, Tenn., doi:10.3334/CDIAC/OTG.PACIFICA_NDP092.
- Tanhua, T., et al. (2008), CARINA data synthesis project, ORNL/CDIAC-157, NDP-091, Carbon Dioxide Information Analysis Center, Oak Ridge Natl. Lab., U. S. Department of Energy, Oak Ridge, Tenn., doi:10.3334/CDIAC/otg.ndp091.
- Tanhua, T., M. Alvarez, and L. Mintrop (2012), Carbon dioxide, hydrographic, and chemical data obtained during the R/V Meteor MT84_3 Mediterranean Sea Cruise (April 5–April 28, 2011), Carbon Dioxide Information Analysis Center, Oak Ridge Natl. Lab., US Department of Energy, Oak Ridge, Tenn., doi:10.3334/CDIAC/OTG.CLIVAR_06MT20110405. [Available at http://cdiac.ornl.gov/ftp/oceans/CLIVAR/Met_84_3_Med_Sea/]
- Wanninkhof, R., J.-Z. Zhang, M. Baringer, C. Langdon, W.-J. Cai, J. Salisbury, and R. Byrne (2011), Carbon dioxide and hydrographic measurements during the 2007 NACP East Coast Cruise Carbon Dioxide Information Analysis Center, Oak Ridge Natl. Lab., U. S. Department of Energy, Oak Ridge, Tenn., doi:10.3334/CDIAC/otg.CLIVAR_NACP_East_Coast_Cruise_2007. [Available at http://cdiac.ornl.gov/ftp/oceans/NACP_East_Coast_Cruise/]
- Wolf-Gladrow, D. A., R. E. Zeebe, C. Klaas, A. Körtzinger, and A. G. Dickson (2007), Total alkalinity: The explicit conservative expression and its application to biogeochemical processes, *Mar. Chem.*, 106(1–2), 287–300, doi:10.1016/j.marchem.2007.01.006.